

X014

## Observation of Shear-wave Splitting from Microseismicity Induced by Hydraulic Fracturing - A Non-VTI Story

P. Kolinsky\* (Microseismic Inc./Institute of Rock Structure and Mechanics), L. Eisner (Microseismic Inc.), V. Grechka (Shell E&P Co.), D. Jurick (Devon Energy Corp.) & P. Duncan (Microseismic Inc.)

### SUMMARY

---

Shear waves from microearthquakes induced by hydraulic fracturing are observed on three-component (3C) accelerometers along a 2 km surface profile. The S-wave waveforms exhibit at least two distinct phases suggesting shear-wave splitting. This observation implies the existence of shear anisotropy between the stimulated reservoir and the surface array. We develop and apply several methods to measure the time delay between the two arrivals. The observed shear-wave splitting suggests that something other than vertical transverse isotropy (VTI) is being encountered at this observation site. This observation may explain why S-waves do not improve location accuracy of microseismic events from surface locations as isotropic or VTI model will not focus S-wave energy recorded at long offsets.

## Introduction

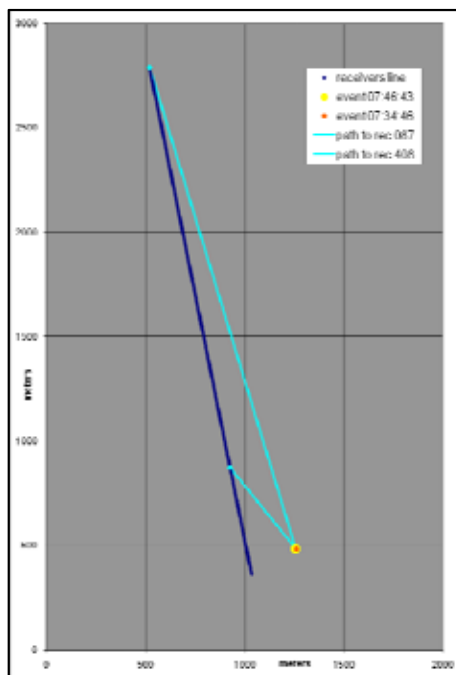


**Figure 1** Map view of the receiver layout. 3C accelerometers are located along the dark blue line, two microseismic events are shown with yellow and orange, schematic ray paths are light blue.

Seismic anisotropy (i.e. the dependence of seismic velocities on the direction of propagation) is commonly observed both in solid earth seismology (upper mantle, core-mantle boundary, inner core) and in seismic prospecting (Thomsen, 1986). In exploration, a proper estimation and handling of anisotropy is helpful for improving reservoir imaging, lithotype discrimination (e.g., shales versus sands), characterizing fractures and stresses, and monitoring the time-lapse changes of producing fields. Additionally, understanding the subsurface anisotropy is crucial for obtaining accurate estimates of induced microseismic event locations.

Inversion for seismic anisotropy remains challenging owing to its multi-parameter nature and the non-uniqueness of typical anisotropy-estimation problems. These are usually overcome by making certain assumptions about the anisotropic symmetry and describing the data within an assumed model such as VTI. To relax those assumptions, we need more data. One option is to supplement conventional P-wave seismic with S-waves (e.g., Teanby et al., 2004). Then, we might observe shear-wave splitting which could help us to constrain the anisotropic symmetries.

In this study, we examine the splitting from induced seismic events recorded along a line of receivers above a hydraulically stimulated reservoir and analyze the implied type of anisotropy. Figure 1 shows the layout of 3C accelerometers relative to the locations of the two largest microseismic events observed during hydraulic treatment of a horizontal well drilled through gas-bearing shale. Seismicity induced by the hydraulic stimulation was found to evolve along narrow east-western trends. The two microseismic events used for this study were induced during the final stage of the stimulation and are located close to each other at true vertical depths around 2125 m.

### Shear-wave picking

The largest microseismic events can be observed on the surface receivers after noise suppression. The long path length between the reservoir and the surface, however, results in significant attenuation of the recorded signals. As attenuation of P- and S-waves is approximately the same per cycle (i.e.  $Q_S \sim Q_P$ ), the S-wave signal at the surface is considerably weaker because the S-waves travel more wavelengths along a similar path. As a result, the useful shear signal in this dataset occurs below 25 Hz. The lower bound of useable frequency content is limited by the background noise. Thus, we had to bandpass the recorded waveforms to a narrow frequency band between 15 Hz and 25 Hz and apply an Automatic Gain Control (AGC) filter.

An additional challenge is posed by the fact that our data are acquired at the surface, which not only distorts direct arrivals but also creates scattered energy of a comparable magnitude. Those multiple arrivals are also observed for P-waves, indicating that multiple shear-wave arrivals result not from multiple anisotropic layers but from near-surface heterogeneity and scattering. Therefore, only the first arrivals of approximately orthogonally polarized S-waves ( $S_1$  and  $S_2$ ) can be confidently picked and used to measure the effective S-wave splitting.

In order to estimate the shear-wave splitting, it is necessary to pick both  $S_1$  and  $S_2$  arrivals. As the source mechanism of microseismic events is unknown, each of these arrivals can have either positive or negative polarity. Given the narrow bandwidth of the waveforms, the arrival picks are subject to a half-period uncertainty. Therefore, we pick the times of the first maxima or minima of the waveforms. Figure 2 gives an example of surface microseismic data acquired during the active well stimulation process.

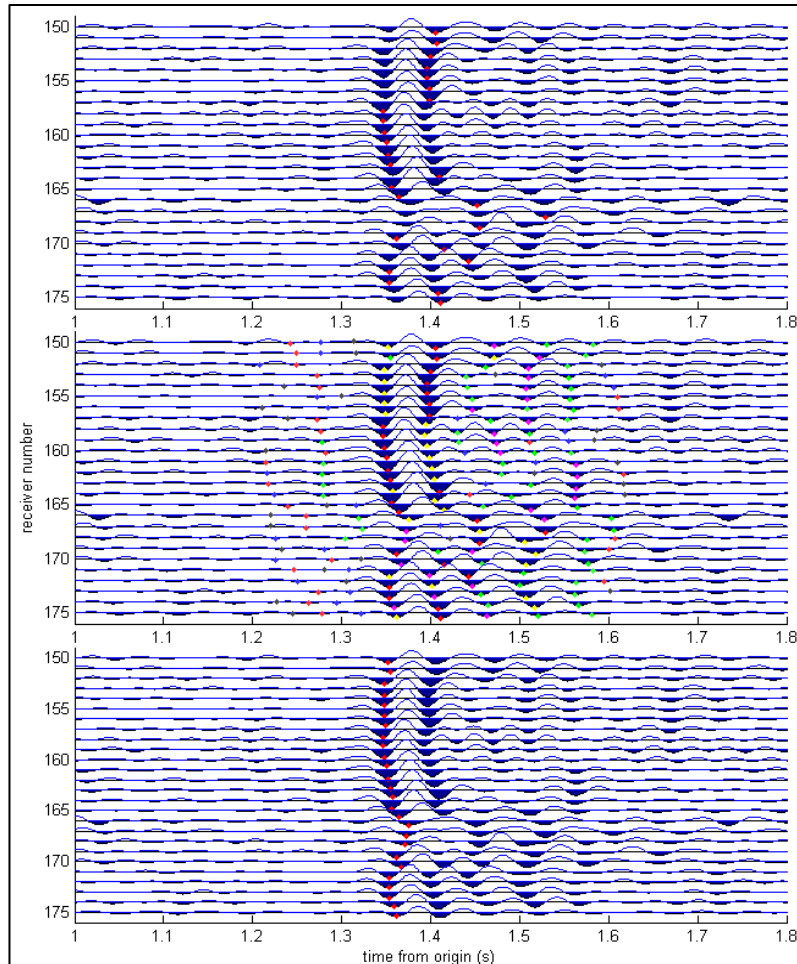


**Figure 2** Radial component of the recorded S-waves. Illustration of the automated picking routine: (top) picks of the maximum peak of each trace; (middle) picks of 8 peaks of each trace; (bottom) smoothed picks of the S-wave arrivals.

To pick the amplitudes automatically, a two-step procedure was developed. First, all peaks and troughs within a preset time interval on each trace along the receiver line are identified. Then we manually select a particular arrival – usually a trace with a high signal-to-noise ratio – and an automatic processing code finds smooth arrival times from adjacent seismograms along the receiver array. We impose a smoothing condition for each receiver as the traveltimes of a seismic wave is expected to be smooth (contrary to the particle polarization which may vary in the presence of near-surface heterogeneities).

Figure 2 illustrates our picking methodology on the radial component of twenty-five receivers in the central position of the receiver line for the peaks only. A time interval of 400 milliseconds is set around the assumed S-wave arrivals. The top plot shows the result of standard picking that selects the largest amplitude at each trace. The middle plot presents picking of eight local peaks. The bottom plot shows a smoothed arrival-time curve compiled by selecting the closest of the eight peaks regardless of their amplitudes.

### Method 1 – assumption of 1D VTI media

Assuming a laterally homogeneous VTI medium, we can rotate the horizontal components into the radial and transverse directions to separate the SV and SH waves based on geometry of each source-receiver pair. We then apply the described semi-automatic picking procedure to the vertical, radial, and transverse components to pick the times of P-, SV- and SH-waves. Unambiguous arrival times were found for hypocentral distances from 2200 to 3220 m. The S-wave splitting measured on the radial and transverse components is shown by the blue line in Figure 3. Note that the SV-wave is faster. The splitting between SV and SH-waves increases with the offset between the distances from 2300 to 2800 m. This increase is consistent

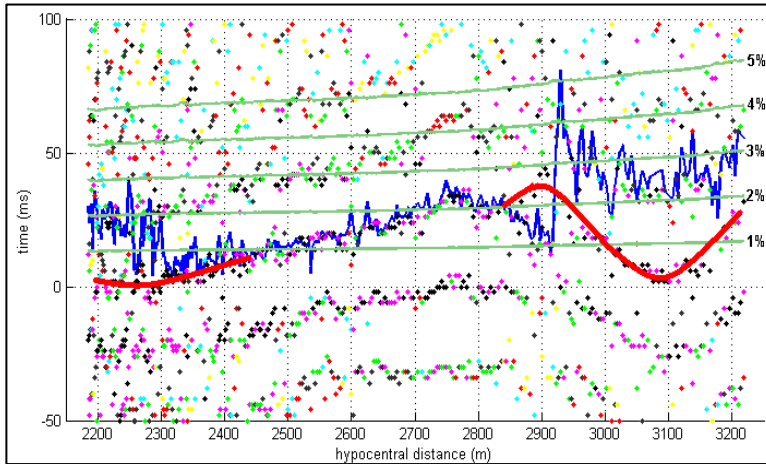


**Figure 3** Arrival time differences between vertically and horizontally polarized S-wave times as functions of the hypocentral distance. Blue line: splitting times between radial (SV) and transverse (SH) waves (positive for faster SV). The red line represent smoothed arrival time differences without assumption of VTI and lateral homogeneity. Dots: splitting times in the horizontal plane by optimal orientation of the components (crosscorrelation); black dots correspond to the maximum of crosscorrelation for each receiver remaining colors represent other peaks. Green lines mark the shear-wave splitting coefficients  $\gamma^{(S)}$  calculated as the ratios of the splitting times to total S-wave times.

studied events. This instability is consistent with our inability to detect any S-wave splitting at near-offset receivers (hypocentral distance less than 2300 m as shown in Figure 3). Thus, we visually inspected the records from some of those receivers and, although the signals were not as strong as at larger offsets, managed to find S-wave splitting such as that shown on the hodogram in Figure 4. The splitting time is significant – approximately 50 ms or nearly 4%. As the splitting observed at near-vertical propagation is greater than that at larger polar angles (Figure 3), it cannot be explained by VTI which requires the splitting to smoothly decrease to zero as the wave-propagation trajectory approaches the vertical and the ray length decreases.

To estimate this more complicated splitting, we introduce a correction to the azimuth by assuming that the S-wave slowness vectors are almost vertical as a result of propagation through a near-surface weathering zone. We then find an optimal orientation of the S-wave polarization locally at each receiver. This is achieved by rotating the horizontal receiver axes in  $1^\circ$  increments and computing the cross-correlation between the rotated horizontal components. The cross-correlation maxima then determine the optimum orientation and the time delay. For this computation, we use the previously estimated S-wave arrival times and limit the search to the time intervals starting approximately one period (50 ms) before and four periods (200 ms) after our time picks. Also, we constrain the rotation to  $\pm 20^\circ$  from the azimuth of the hypocenter. Figure

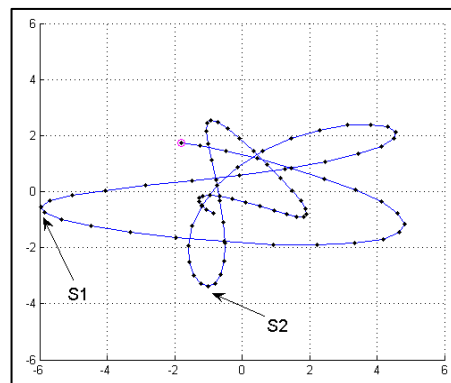


**Figure 4** Particle motion in the horizontal plane. Hodogram of 50 ms around the first S-wave arrival at receiver 52 is shown. Red circle denotes the beginning of the particle motion. Each black dot represents 2 ms.

3 shows the splitting times obtained with cross-correlation for each receiver by colored dots corresponding to the different maxima of the cross-correlation function. For the hypocentral distance from 2300 m to 2800 m, one of the cross-correlation maxima coincides with the previously estimated splitting from Method 1 (blue line). Method 2, however, seems to extend the splitting measurements to a larger range of offsets (red line). Figure 5 shows an example

with a VTI media as the SH-wave can travel slower than the SV-wave at intermediate polar angles (Thomsen, 2002).

### Method 2 – assumption of vertical S-wave slowness vectors

The event arrivals in Figure 2 indicate a significant near-surface scattering. It is very likely that this scattering causes deviation of the laterally refracted S-waves from the directions to hypocenter. Furthermore, at small offsets, the estimated hypocenter azimuthal directions are severely compromised by lateral errors in the estimated locations of the

of the optimally rotated receiver components and the time-shifted waveforms of two approximately orthogonally polarized S-waves.

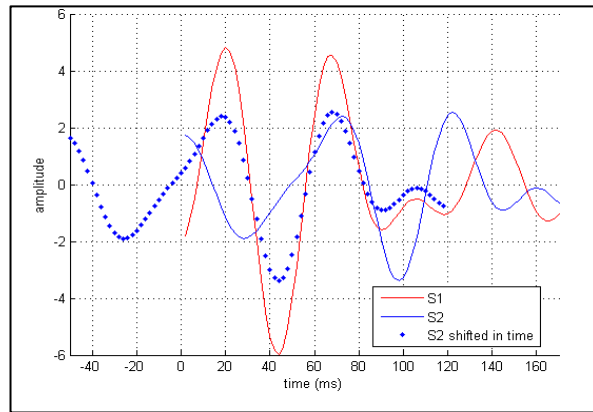


**Figure 5** Example of splitting on receiver 52. Red line is the optimally oriented horizontal fast S-component, solid blue line is the slow S-component, and dotted blue line is the slow S-trace optimally shifted to fit the fast S-wave. The estimated splitting is 50 ms.

### Discussion and conclusions

We observed S-wave splitting on 3C accelerometers that recorded microseismic events induced by hydraulic fracture well stimulation. Although VTI symmetry can explain the splitting of shear-waves at distances between 2300 m and 2800 m, a careful inspection of the S-wave particle motions reveals a greater splitting at near-vertical propagation. This observation provides evidence for a possible non-VTI type of anisotropy. In fact, this finding is not that surprising since shear-wave splitting is usually observed in multicomponent zero-offset VSP data (Winterstein et al., 2001). The shear-wave time delay of about 25 ms

measured at the hypocentral distance of 2800 m (or at the offset-to-depth ratio equal to 0.85) yields the shear-wave splitting coefficient  $\gamma^{(S)}$  of approximately 2% (or 4% if the half-period uncertainty is included). The time delay at the small-offset receivers is close to 50 ms corresponding to  $\gamma^{(S)} \approx 4\%$ . This conclusion has an important implication for location of microseismic events: without the knowledge of type and strength of anisotropy, the S-waves do not improve location accuracy as the S-wave energy does not focus at the hypocenter.

Finally, the vertical stratigraphic section between 1500 m and 2100 m in a well in this reservoir was logged with a dipole sonic tool, which does not show any significant shear wave anisotropy in the vertical direction. To explain this discrepancy, we have to suppose that either the S-wave splitting mostly occurs in the subsurface above 1500 m (as observed by Winterstein et al., 2001) or the anisotropy is frequency dependent and the sonic logging frequencies (2-20 kHz) measure different rock properties than those sensed by surface seismic data.

### Acknowledgements

We would like to thank Devon Energy for releasing of this dataset for publication.

### References

Teanby, N., J.-M. Kendall, R.H. Jones, and O. Barkved [2004] Stress-induced temporal variations in seismic anisotropy observed in microseismic data, *Geophys. J. Int.* (2004) 156, 459–466.

Thomsen, L. [1986] Weak elastic anisotropy. *Geophysics*, Vol. 51, No. 10, 1954-1966.

Thomsen, L. [2002] Understanding Seismic Anisotropy in Exploration and Exploitation. Distinguished Instructor Short Course, *Distinguished instructor Series*, No. 5, SEG, EAGE.

Winterstein, D. F., G. S. De and M. A. Meadows [2001] Twelve years of vertical birefringence in nine-component VSP data: *Geophysics*, Vol. 66, 582–597.